Non-Hermitian higher-order topological states in nonreciprocal and reciprocal systems with their electric-circuit realization

Motohiko Ezawa

Phys. Rev. B **99**, 201411 — Published 21 May 2019

DOI: 10.1103/PhysRevB.99.201411

Non-Hermitian higher-order topological states in nonreciprocal and reciprocal systems with their electric-circuit realization

Motohiko Ezawa
Department of Applied Physics, University of Tokyo, Hongo 7-3-1, 113-8656, Japan

A prominent feature of some one-dimensional non-Hermitian systems is that all right-eigenstates of the non-Hermitian Hamiltonian are localized in one end of the chain. The topological and trivial phases are distinguished by the emergence of zero-energy modes within the skin states in the presence of the chiral symmetry. Skin states are formed when the system is nonreciprocal, where it is said nonreciprocal if the absolute values of the right- and left-going hoppings amplitudes are different. Indeed, the zero-energy edge modes emerge at both edges in the topological phase of the reciprocal non-Hermitian system. Then, analyzing higher-order topological insulators in nonreciprocal systems, we find the emergence of topological zero-energy modes within the skin states formed in the vicinity of one corner. Explicitly we explore the anisotropic honeycomb model in two dimensions and the diamond lattice model in three dimensions. We also study an electric-circuit realization of these systems. Electrical circuits with (without) diodes realize the nonreciprocal (reciprocal) non-Hermitian topological systems. Topological phase transitions are observable by measuring the impedance resonance due to zero-admittance topological corner modes.

Introduction: Topological physics is one of the most important achievements in contemporary physics, among which there are topological insulators and its generalization to higher-order topological insulators[1–12]. They are characterized by the bulk topological numbers, where the bulk-boundary correspondence and its generalization play a key role. In particular, topological zero-energy corner modes emerge for the second-order topological insulators in two dimensions and for the third-order topological insulators in three dimensions. They have been studied not only in condensed matter physics but also in various systems such as photonic[13–15], phononic[16–20] and microwave[21,22] systems. LC electric circuits have also topological phases[23–28].

Recently, non-Hermitian topological systems attract increasing attentions[29–42]. They are realized in photonic systems[43–46], microwave resonators[47], wave guides[48], quantum walks[49,50] and cavity systems[51]. Non-Hermitian generalizations of the Su-Schrieffer-Heeger (SSH) model have been most studied[33,35–37,44,46,47,52,53]. Non-Hermitian systems have new aspects. First, we must differentiate between the right and left eigenenergies and eigenstates, which are defined by $H\left|\psi^{\mathrm{R}}\right\rangle = \varepsilon^{\mathrm{R}}\left|\psi^{\mathrm{R}}\right\rangle$ and $H^{\dagger}\left|\psi^{\mathrm{L}}\right\rangle = \varepsilon^{\mathrm{L}}\left|\psi^{\mathrm{L}}\right\rangle$. The right and left eigenenergies are complex in general. A prominent property of some non-Hermitian systems is the non-Hermitian skin effect, where all right-eigenstates are localized in one end of a finite chain with the bulk spectrum being totally modified[37,38,53–56]. An interesting feature is that the topological phase transition point for a finite system is different from the bulk gap closing point. The topological and trivial phases are distinguished by the presence of the zero-energy edge mode within the skin states. The topological number is given by the so-called non-Bloch topological invariant[37,57,58], which well describes the phase transition point for a finite system.

In this work, first we clarify the condition for the skin states to develop in the non-Hermitian SSH model. The condition is found to be the nonreciprocity of the hopping between the lattice sites. We then generalize the analysis to higher dimensions. The Hermitian SSH model has been generalized to higher dimensions such the anisotropic honeycomb and diamond lattice models, where they are shown to be higher-order topological insulators[2,4–6,9,59]. We investigate nonreciprocal versions of these models, and demonstrate the emergence of the topological corner modes within the skin states: See Fig.1.

Electric circuits realize various topological phases[23–28]. We show that LCR circuits with (without) diodes present a concrete playground to investigate nonreciprocal (reciprocal) non-Hermitian topological physics (see Fig.2), where resistors naturally lead to non-Hermitian terms and diodes to nonreciprocal terms. We focus on the chiral symmetric topological electric circuits. When we analyze the SSH model, the anisotropic honeycomb and diamond lattice models in LC circuits, there are many impedance resonances both in the topological and trivial phases. All of them are drastically suppressed except for the topological zero-admittance modes due to the effect of resistors in LCR circuits. We then investigate their nonreciprocal versions by introducing diodes, and conclude that the emergence of topological corner modes in skin states is clearly detectable by impedance peaks.

Non-Hermitian minimal two-band models: The minimal model to describe insulators is the two-band model. Indeed, one-band model cannot have a line gap to generate insulators although it is possible to have a point gap[60]. The unit cell contains two sites A and B, and it is called a bipertite system. We investigate the chiral symmetric model since it is known to have nontrivial topology protected by the symmetry. The model is described by the 2×2 Hamiltonian H, which is expanded in terms of the Pauli matrices,

$$H\left(\boldsymbol{k}\right) = \begin{pmatrix} 0 & h_1\left(\boldsymbol{k}\right) \\ h_2\left(\boldsymbol{k}\right) & 0 \end{pmatrix}. \tag{1}$$

It has the chiral symmetry σ_z satisfying $\left\{H\left(\boldsymbol{k}\right),\sigma_z\right\} = 0$, which assures the symmetric spectrum $E \leftrightarrow -E$. The diagonal terms are prohibited by the chiral symmetry. Typical examples are the SSH model in one dimension, the anisotropic honeycomb lattice in two dimensions, and the anisotropic diamond lattice in three dimensions. See Figs.1 and 2 for illustrations of these lattices and also the corresponding electric

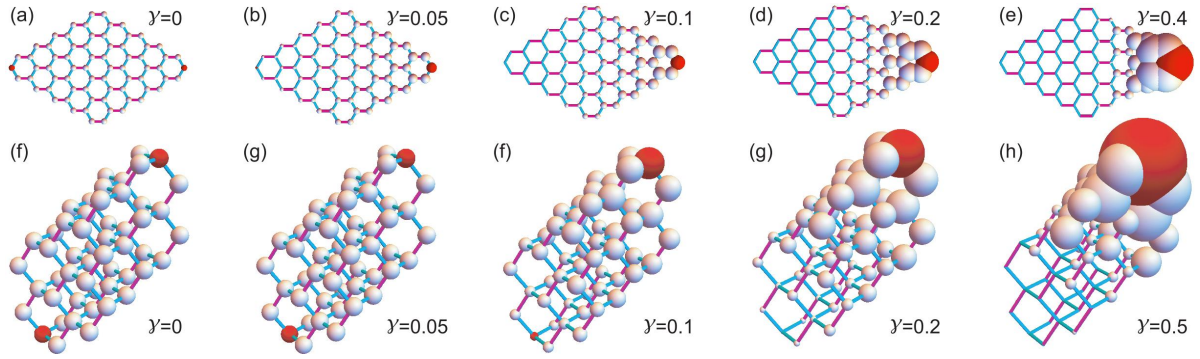

FIG. 1: (a)–(e) Development of the skin states (in gold) and the topological corner modes (in red) in rhombus geometry of the nonreciprocal honeycomb system as the nonreciprocity γ increases. The size of a ball represents the magnitude of LDOS. We have set $t_A = 0.4$ and $t_B = 1$. (f)–(h) The corresponding ones in rhombohedron geometry of the diamond lattice system. We have set $t_A = 0.5$ and $t_B = 1$.

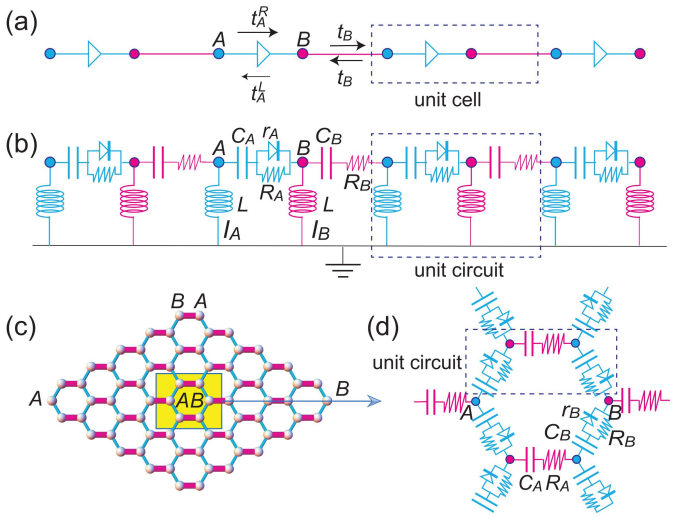

FIG. 2: (a) Illustration of the SSH model. One unit cell contains two sites A and B. Nonreciprocal links are shown by the symbol $\triangleright$. (b) Illustration of the SSH circuit. The reciprocal link is represented by a condenser and a resistance connected in series. The nonreciprocal link is obtained by replacing this resistance with a set of a diode and a resistance connected in parallel. (c) Illustration of the anisotropic honeycomb model. (d) Illustration of the electric-circuit realization. Each node is connected to the ground via inductance L as in (b).

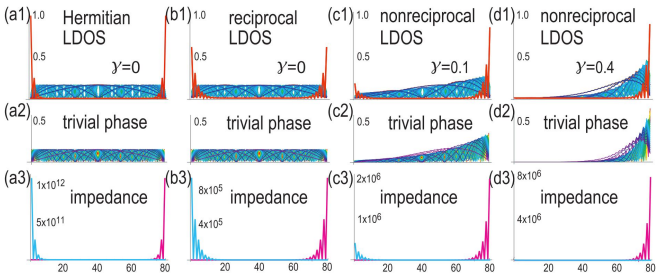

FIG. 3: LDOS in the topological and trivial phases of the SSH model for (a1)–(d1) and (a2)–(d2), respectively. The horizontal axis denotes the lattice site number. Red curves represent the topological edge modes in (a1)–(d1). (a1) LDOS of the Hermitian system, where the topological edge modes are prominent at both edges. (b1) LDOS of the reciprocal non-Hermitian system, which is quite similar to that of the Hermitian system. (c1)–(d1) LDOS of the nonreciprocal non-Hermitian system, where the skin states are formed. (a3)–(d3) Impedance (in unit of Ω) in the corresponding SSH circuits. We have taken $t_A = 0.25$, $t_B = 1$ and $\gamma = 0$ for (a), $t_A = 0.25 + 0.5i$, $t_B = 1 + 0.5i$ and $\gamma = 0$ for (b), while $t_A = 0.25 + 0.5i$, $t_B = 1 + 0.5i$ and $\gamma = 0.1$ for (c) while $t_A = 0.25 + 0.5i$, $t_B = 1 + 0.5i$ and $\gamma = 0.4$ for (d).

circuits. It is non-Hermitian when $h_2(\boldsymbol{k}) \neq h_1^*(\boldsymbol{k})$.

The quantum mechanical Hamiltonian describes hopping between two adjacent sites. When the absolute value of the hopping toward one direction is equal to the one toward the opposite direction, the system is said reciprocal and otherwise nonreciprocal. It is intriguing that the hopping amplitude may be complex. Indeed, complex hopping parameters appear naturally in an electric-circuit realization of the non-Hermitian systems: See Eq.(6). We have reciprocal and nonreciprocal non-Hermitian systems.

Non-Hermitian SSH models: We start with the non-Hermitian SSH model[36,37,53], where $h_1(k) = t_A^L + t_B e^{-ik}$ and $h_2(k) = t_A^R + t_B e^{ik}$. We illustrate the hopping parameters in Fig.2(a) and they are complex in general. The system is reciprocal for $|t_A^L| = |t_A^R|$, and nonreciprocal otherwise. Let us set $t_A^L = t_A + \gamma/2$, $t_A^R = t_A - \gamma/2$, and call γ the nonreciprocity.

The topological and trivial phases are distinguished by the emergence of zero-energy edge modes for a finite chain. We define the local density of states (LDOS) for the n-th right-eigen state $|\psi_n^{\mathrm{R}}(x)\rangle$ by $\left||\psi_n^{\mathrm{R}}(x)\rangle\right|^2$. We show the LDOS for all n with a choice of typical values of hopping parameters for a finite chain in Fig.3. (i) The Hermitian SSH model is described by taking a real parameter, $t_A \equiv t_A^L = t_A^R$. There are zero-energy modes at both edges in the topological phase with $|t_A| < |t_B|$ but none in the trivial phase with $|t_A| > |t_B|$: See Fig.3(a1)–(a2). (ii) We consider the reciprocal non-Hermitian system by taking a complex value for $t_A = t_A^L = t_A^R$. As in Fig.3(b1), the LDOS is quite similar to the Hermitian SSH model though the bulk energy becomes complex. The phase transition point is the same, i.e., at $|t_A| = |t_B|$. (iii) In

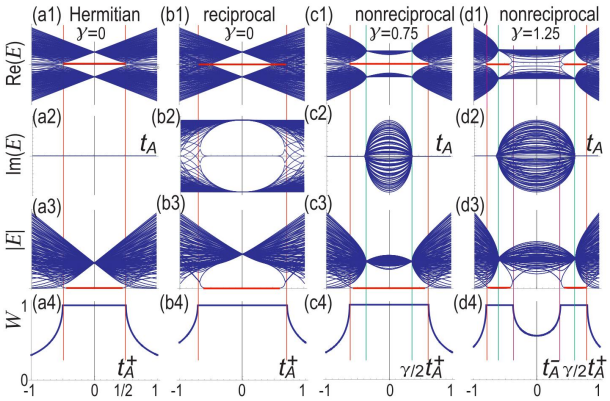

FIG. 4: Energy spectra and topological numbers of the rhombus made of the anisotropic honeycomb lattice. The horizontal axis is t_A, while the vertical axis is the real part of the energy for (*1), the imaginary part for (*2), the absolute value for (*3), and the topological number W for (*4). The horizontal red lines represent the topological corner modes, where the system is a second-order topological insulator. (a*) for the Hermitian model, (b*) for the reciprocal non-Hermitian model, (c*)–(d*) for the nonreciprocal non-Hermitian model with increasing γ. The vertical lines represent the phase transition points at the value t_A^+ (magenta), t_A^- (violet) and $\gamma/2$ (green). We have taken $t_B = 1$ for (a), $t_B = 1 + i$ for (b), $t_B = 1$ for (c), $t_B = 1$ for (d).

Fig.3(c1)–(d1), we show the LDOS for the nonreciprocal non-Hermitian system[37] with $|t_A^L| \neq |t_A^R|$, which demonstrates the formation of the skin states. By examining the zero-energy edge mode, the system is topological for $\left|t_A^L t_A^R\right| < |t_B|^2$ and trivial for $\left|t_A^L t_A^R\right| > |t_B|^2$. Skin states are induced by the nonreciprocity both in the topological and trivial phases. The zero-energy mode emerges only at one edge in the topological phase. This is called the biorthogonal bulk-boundary correspondence[37,53]. We present some analytic formulas to understand the LDOS elsewhere[61].

Non-Bloch winding numbers: The non-Bloch topological number[37,57,58] describes the nonreciprocal non-Hermitian SSH model. Here, we use the chiral index Γ as the non-Bloch topological number. It is defined by[62]

$$\Gamma = \frac{1}{2i}\int_{-\pi}^{\pi}\frac{dk}{2\pi}\mathrm{Tr}\left[\sigma_z H\left(k+i\kappa\right)^{-1}\partial_k H\left(k+i\kappa\right)\right] \quad (2)$$

in the two-band model (1), where $\kappa = -\log\sqrt{\left|t_A^R/t_A^L\right|}$. It is zero, $\kappa = 0$, for the reciprocal system, where this formula is reduced to the usual chiral index. It is quantized as long as the chiral symmetry is preserved. In addition, it cannot change its value as long as the Hamiltonian is not singular. To see this, by substituting (1) to (2), we obtain

$$\Gamma = \frac{1}{2}\int_{-\pi}^{\pi}\frac{dk}{2\pi i}\partial_k \log[h_2(k+i\kappa)/h_1(k+i\kappa)]. \quad (3)$$

Hence, the chiral index counts how many times the Hamiltonian winds the origin. By evaluating it, we find that the system is topological ($\Gamma = 1$) for $\left|t_A^L t_A^R\right| < |t_B|^2$ and trivial ($\Gamma = 0$) for $\left|t_A^L t_A^R\right| > |t_B|^2$, as agrees with the condition for the zero-energy edge modes to emerge in the skin states.

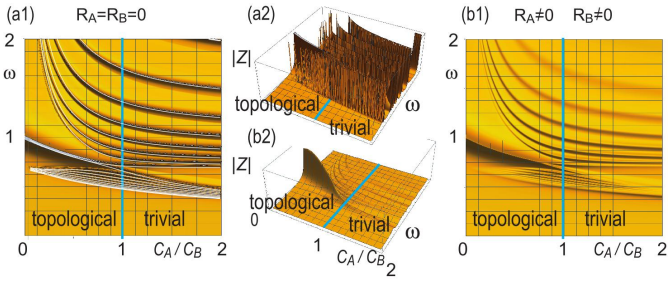

FIG. 5: Impedance peaks are shown in the (C_A/C_B)-ω plane. Phase transition occurs at $C_A = C_B$. (a) Many impedance peaks are generated as implied by Eq.(8) both in the topological and trivial phases of the Hermitian SSH model ($R_A = R_B = 0$). White curves represent the analytical result (8). (b) All these peaks are suppressed drastically except for the topological peak in the topological phase of the reciprocal non-Hermitian SSH model ($R_A \neq 0, R_B \neq 0$).

A comment is in order. Although the chiral index (2) has a different expression from the non-Bloch topological number defined in Ref.[37], it is shown[62] that they are equivalent.

Non-Hermitian honeycomb lattices: We proceed to investigate non-Hermitian systems in two dimensions. A typical example is the anisotropic honeycomb lattice model illustrated in Fig.2(c). The nonreciprocal hopping is introduced as explained in Fig.2(d). The Hamiltonian is given by the 2×2 matrix (1) with $h_1 = 2t_A^L\cos(k_y/2) + t_B\exp(-ik_x)$ and $h_2 = 2t_A^R\cos(k_y/2) + t_B\exp(ik_x)$. The chiral index (2) is generalized to D dimensions as

$$\Gamma = \frac{1}{2i}\int\frac{d^D\boldsymbol{k}}{(2\pi)^D}\mathrm{Tr}\left[\sigma_z H\left(\boldsymbol{k}+i\boldsymbol{\kappa}\right)^{-1}\partial_{k_x} H\left(\boldsymbol{k}+i\boldsymbol{\kappa}\right)\right], \quad (4)$$

where the integration is performed over the Brillouin zone with $\boldsymbol{\kappa} = (\kappa, \boldsymbol{0})$. It is quantized when the system is an insulator, while it changes its value continuously when the system is metal. The system is topological for $\left|t_A^L t_A^R/t_B^2\right| < 1$. The topological phase transition occurs from a topological insulator to a metal at $t_A^+ = \pm\frac{1}{2}\sqrt{|t_B|^2+\gamma^2}$ for $|t_B| > |\gamma|$. On the other hand, there are additional topological phase transitions at $t_A^- = \pm\frac{1}{2}\sqrt{-|t_B|^2+\gamma^2}$ for $|t_B| < |\gamma|$: See Fig.4. We give the derivation of $t_A^\pm$ elsewhere[63].

We show the energy spectra and the topological numbers for various values of hopping parameters for a rhombus made of the anisotropic honeycomb lattice in Fig.4. (i) The Hermitian model is described by a real value for $t_A = t_A^L = t_A^R$. The Hermitian model produces a second-order topological insulator in the parameter region $|t_A/t_B| < 1/2$. Namely, when we consider a nanoribbon, there are no topological edge modes. On the other hand, topological corner modes emerge at two corners in a rhombus as in Fig.1(a). These corner modes are observed as zero-energy modes (depicted in red lines) in Fig.4(a). (ii) The reciprocal non-Hermitian system is constructed by taking a complex value for $t_A = t_A^L = t_A^R$. The structure of the real part of the energy spectrum and the

topological charge are quite similar to those of the Hermitian model, though the energy becomes complex as in Fig.4(b2). (iii) We consider the nonreciprocal non-Hermitian systems in Fig.4(c) and (d). The zero-energy corner mode emerges at one of two corners in a rhombus, as is found by calculating the LDOS: See Fig.1. These corner modes are observed as zero-energy modes (depicted in red lines) in Fig.4(c) and (d).

In the similar way, we may analyze the skin states and the topological corner mode in rhombohedron geometry of the diamond lattice. The Hamiltonian is given by the 2×2 matrix (1) with $h_1 = t_A^L\left(2\cos(k_y/2) + \exp\left(-ik_z\right)\right) + t_B\exp(-ik_x)$ and $h_2 = t_A^R\left(2\cos(k_y/2) + \exp\left(ik_z\right)\right) + t_B\exp(ik_x)$. The lattice structure is illustrated in Fig.1, where the nonreciprocity is introduced just as in Fig.2(d). The LDOS is also shown in Fig.1, which demonstrates the formation of skin states and the topological corner mode. It is a typical example of the nonreciprocal third-order topological insulators in three dimensions[64].

Electric-circuit realization of non-Hermitian systems: We consider a class of electric circuits, where each node a is connected to the ground via inductance L: See Fig.2(b). Let I_a be the current between node a and the ground via the inductance, V_a be the voltage at node a, C_{ab} and R_{ab} be the capacitance and the resistance connected in series between nodes a and b, respectively. We use diodes to implement nonreciprocity in the circuit. We approximate a diode by a linear resistance r_{ab} for $a < b$ and the perfect nonreciprocity $r_{ab} = \infty$ for $b < a$. We set $C_{AB} = C_A$, $C_{BA} = C_B$, $R_{AB}^R = r_A R_A/(r_A + R_A)$, $R_{AB}^L = R_A$, $R_{BA}^R = R_{BA}^L = R_B$ in a bipertite system.

The Kirchhoff's current law leads to the circuit Laplacian[23,24] $J_{ab}(\omega)$ with ω the frequency,

$$J_{ab}\left(\omega\right) = i\omega\delta_{ab}[-\frac{1}{\omega^2 L} + \sum_{c\neq a} H_{ac}(\omega)] - i\omega H_{ab}\left(\omega\right), \quad (5)$$

where $H_{ab}\left(\omega\right) = C_{ab}/\left(1 + i\omega C_{ab}\bar{R}_{ab}\right)$. Here, $\bar{R}_{ab} = R_{ab}$ for $a > b$, $\bar{R}_{ab} = r_{ab}R_{ab}/(r_{ab}+R_{ab})$ for $a < b$, and $C_{aa} = 0$ and $\bar{R}_{aa} = 0$. An important observation is that $H_{ab}\left(\omega\right)$ is identified as the tight-binding Hamiltonian in condensed-matter physics, where the hopping parameters between adjacent sites a and b are given by

$$\begin{aligned} &t_A^L = C_A/\left(1 + i\omega C_A R_A\right), \quad t_B = C_B/\left(1 + i\omega C_B R_B\right), \\ &t_A^R = C_A/[1 + i\omega C_A/\left(1/R_A + 1/r_A\right)]. \end{aligned} \quad (6)$$

The hopping parameters become complex.

Admittance spectrum and impedance peaks: The admittance spectrum consists of the eigenvalues of the circuit Laplacian[23–28]. It is identical to the band structure in condensed-matter physics. Thus, the topological edge or corner modes correspond to the zero-admittance modes.

A measurable quantity of electric circuits is the impedance, which is given by[26] $G_{ab} = V_a/I_b$, where G is the green function defined by the inverse of the Laplacian J, $G \equiv J^{-1}$. It diverges at the frequency satisfying $J = 0$. Therefore, it is possible to detect the topological zero-admittance modes by the divergence of the impedance.

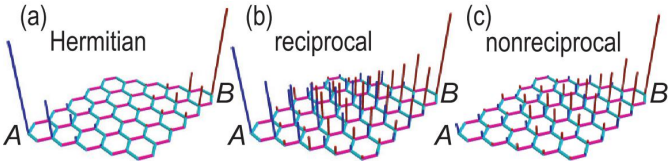

FIG. 6: Spatial distribution of impedance in the topological phase of the anisotropic honeycomb circuit. (a) In the Hermitian system, enhanced topological peaks emerge at both corners. (b) In the reciprocal non-Hermitian system topological peaks emerge at both corners, but they are not so prominent. (c) In the nonreciprocal system, an enhanced topological peak emerges only at corner B corresponding to the topological skin corner states around corner B as in Fig.2.

Let us first search for zero-admittance modes in the LC circuit. After the diagonalization, the circuit Laplacian reads

$$J_n\left(\omega\right) = i\omega[-(\omega^2 L)^{-1} + \sum_{\alpha=A,B} n_\alpha C_\alpha] - i\omega\varepsilon_n\left(\omega\right), \quad (7)$$

where n_α is the number of the nodes adjacent to node α, and ε_n is the eigenvalue of the circuit Laplacian. The impedance diverges at the resonance frequencies

$$\omega_{\mathrm{R}}(\varepsilon_n) = \sqrt{(-\varepsilon_n + \sum_\alpha n_\alpha C_\alpha)/L}, \quad (8)$$

which is the solution of $J_n\left(\omega\right) = 0$. Hence there are many impedance peaks indexed by n both in the topological and trivial phases as in Fig.5(a1)–(a2) for the instance of the SSH model, among which the topological impedance peak is given by the zero-admittance mode ($\varepsilon_0 = 0$) in the topological phase. However, when we introduce resistors, since ε_n becomes complex except for the zero-admittance mode ($\varepsilon_0 = 0$), all resonance peaks are drastically suppressed except for the topological peak as in Fig.5(b1)–(b2) for the instance of the SSH model. This phenomenon occurs in any dimensions, since the resonance frequency (8) is valid in any dimensions.

We first present calculate the impedance at each node in the SSH model. We show a space distribution of the point impedance in the topological phase in Fig.3(a3)–(d3). We see how the topological impedance peak develops in the skin states as the nonreciprocity γ increases.

We next calculate the impedance at each node in rhombus (rhombohedron) geometry of the anisotropic honeycomb (diamond) lattice, where the second-order (third-order) topological phase is realized and the topological corner mode emerges. We show a space distribution of the point impedance in the topological phase in Fig.6(a), (b) and (c) for the Hermitian, reciprocal non-Hermitian and nonreciprocal non-Hermitian honeycomb systems, respectively. In the reciprocal system, impedance peaks emerge at corners A and B. On the other hand, in the nonreciprocal system, an impedance peak emerges only at corner B corresponding to the topological corner modes in Fig.1.

Discussion: We have studied a non-Hermitian extension of the higher-order topological phases and proposed to realize

them by electric circuits. Our results show that various non-Hermitian systems will be implimented in electric circuits.

After submission of this work, we find closely related works[65–67] on the non-Hermitian extensions of the higher-order topological phases.

The author is very much grateful to N. Nagaosa for helpful discussions on the subject. This work is supported by the Grants-in-Aid for Scientific Research from MEXT KAKENHI (Grants No. JP17K05490, No. JP15H05854 and No. JP18H03676). This work is also supported by CREST, JST (JPMJCR16F1 and JPMJCR1874).

[1] F. Zhang, C.L. Kane and E.J. Mele, Phys. Rev. Lett. **110**, 046404 (2013).
[2] W. A. Benalcazar, B. A. Bernevig, and T. L. Hughes, 10.1126/science.aah6442.
[3] F. Schindler, A. Cook, M. G. Vergniory, and T. Neupert, in APS March Meeting (2017).
[4] Y. Peng, Y. Bao, and F. von Oppen, Phys. Rev. B **95**, 235143 (2017).
[5] J. Langbehn, Y. Peng, L. Trifunovic, F. von Oppen, and P. W. Brouwer, Phys. Rev. Lett. **119**, 246401 (2017).
[6] Z. Song, Z. Fang, and C. Fang, Phys. Rev. Lett. **119**, 246402 (2017).
[7] W. A. Benalcazar, B. A. Bernevig, and T. L. Hughes, Phys. Rev. B **96**, 245115 (2017).
[8] F. Schindler, A. M. Cook, M. G. Vergniory, Z. Wang, S. S. P. Parkin, B. A. Bernevig, and T. Neupert, Science Advances 4, eaat0346 (2018).
[9] M. Ezawa, Phys. Rev. Lett. 120, 026801 (2018).
[10] F. Schindler, Z. Wang, M. G. Vergniory, A. M. Cook, A. Murani, S. Sengupta, A. Y. Kasumov, R. Deblock, S. Jeon, I. Drozdov, H. Bouchiat, S. Gueron, A. Yazdani, B. A. Bernevig, and T. Neupert, Nat. Physics 14, 918 (2018).
[11] E. Khalaf, H. C. Po, A. Vishwanath and H. Watanabe, Phys. Rev. X 8, 031070 (2018).
[12] M. Ezawa, Phys. Rev. Lett. 121, 116801 (2018).
[13] L. Lu, J. D. Joannopoulos and M. Soljacic, Nat. Photon 8, 821 (2014).
[14] N. Goldman, J. C. Budich, P. Zoller, Nat. Phys. 12, 639 (2016).
[15] B. Y. Xie, H. F. Wang, H.-X. Wang, X. Y. Zhu, J.-H. Jiang, M. H. Lu, Y. F. Chen, Phys. Rev. B 98, 205147 (2018).
[16] R. Susstrunk, S. D. Huber, Science 349, 47 (2015).
[17] Z. Yang, F. Gao, X. Shi, X. Lin, Z. Gao, Y. Chong and B. Zhang, Phys. Rev. Lett. 114, 114301 (2015).
[18] M. S.-Garcia, V. Peri, R. Susstrunk, O. R. Bilal, T. Larsen, L. G. Villanueva, S. D. Huber, Nature 555, 342 (2018).
[19] H. Xue, Y. Yang, F. Gao, Y. Chong and B. Zhang, Nature Materials 18, 108 (2019).
[20] X. Ni, M. Weiner, A. Alu, and A. B. Khanikaev, Nature Materials 18, 113 (2019).
[21] W. Hu, J. C. Pillay, K. Wu, M. Pasek, P. P. Shum, and Y. D. Chong, Phys. Rev. X 5, 011012 (2015).
[22] C. W. Peterson, W. A. Benalcazar, T. L. hughes and G. Bahl, Nature 555, 346 (2018).
[23] C. H. Lee , S. Imhof, C. Berger, F. Bayer, J. Brehm, L. W. Molenkamp, T. Kiessling and R. Thomale, Communications Physics, 1, 39 (2018).
[24] S. Imhof, C. Berger, F. Bayer, J. Brehm, L. Molenkamp, T. Kiessling, F. Schindler, C. H. Lee, M. Greiter, T. Neupert, R. Thomale, Nat. Phys. 14, 925 (2018).
[25] M. Serra-Garcia, R. Susstrunk and S. D. Huber, Phys. Rev. B 99, 020304 (2019).
[26] T. Helbig, T. Hofmann, C. H. Lee, R. Thomale, S. Imhof, L. W. Molenkamp and T. Kiessling, Phys. Rev. B 99, 161114 (2019).
[27] Y. Lu, N. Jia, L. Su, C. Owens, G. Juzeliunas, D. I. Schuster and J. Simon, Phys. Rev. B 99, 020302 (2019).
[28] M. Ezawa, Phys. Rev. B 98, 201402(R) (2018).
[29] C. M. Bender and S. Boettcher, Phys. Rev. Lett. 80, 5243 (1998).
[30] C. M. Bender, D. C. Brody, and H. F. Jones, Phys. Rev. Lett. 89, 270401 (2002).
[31] V. V. Konotop, J. Yang, and D. A. Zezyulin, Rev. Mod. Phys. 88, 035002 (2016).
[32] R. El-Ganainy, K. G. Makris, M. Khajavikhan, Z. H. Musslimani, S. Rotter and D. N. Christodoulides, Nat. Physics 14, 11 (2018).
[33] T. E. Lee, Phys. Rev. Lett. 116, 133903 (2016).
[34] T. Rakovszky, J. K. Asboth, and A. Alberti, Phys. Rev. B 95, 201407(R) (2017).
[35] S. Lieu, Phys. Rev. B 97, 045106 (2018).
[36] C. Yin, H. Jiang, L. Li, Rong Lu and S. Chen, Phys. Rev. A 97, 052115 (2018).
[37] S. Yao and Z. Wang, Phys. Rev. Lett. 121, 086803 (2018).
[38] L. Jin and Z. Song, Phys. Rev. B 99, 081103 (2019).
[39] S.-D. Liang and G.-Y. Huang, Phys. Rev. A 87, 012118 (2013).
[40] D. Leykam, K. Y. Bliokh, Chunli Huang, Y. D. Chong, and Franco Nori, Phys. Rev. Lett. 118, 040401 (2017).
[41] H. Shen, B. Zhen and L. Fu Phys. Rev. Lett. 120, 146402 (2018).
[42] H. Menke and M. M. Hirschmann, Phys. Rev. B 95, 174506 (2017).
[43] K. G. Makris, R. El-Ganainy, D. N. Christodoulides, and Z. H. Musslimani, Phys. Rev. Lett. 100, 103904 (2008).
[44] H. Schomerus, Opt. Lett. 38, 1912 (2013).
[45] M. Pan, H. Zhao, P. Miao, S. Longhi, and L. Feng, Nat. Commun. 9, 1308 (2018).
[46] S. Weimann, M. Kremer, Y. Plotnik, Y. Lumer, S.Nolte, K. G. Makris, M. Segev, M. C. Rechtsman, and A. Szameit, Nat. Mater. 16, 433 (2017).
[47] C. Poli, M. Bellec, U. Kuhl, F. Mortessagne and H. Schomerus, Nat. Com. 6, 6710 (2015).
[48] J. M. Zeuner, M. C. Rechtsman, Y. Plotnik, Y. Lumer, S. Nolte, M. S. Rudner, M. Segev, and A. Szameit, Phys. Rev. Lett. 115, 040402 (2015).
[49] M. S. Rudner and L. S. Levitov, Phys. Rev. Lett. 102, 065703 (2009).
[50] L. Xiao, X. Zhan, Z. H. Bian, K. K. Wang, X. Zhang, X. P. Wang, J. Li, K. Mochizuki, D. Kim, N. Kawakami, W. Yi, H. Obuse, B. C. Sanders, and P. Xue, Nat. Physics 13, 1117 (2017).
[51] H. Hodaei, A. U Hassan, S. Wittek, H. Garcia-Gracia, R. El-Ganainy, D. N. Christodoulides and M. Khajavikhan, Nature 548, 187 (2017).
[52] B. Zhu, R. Lu and S. Chen, Phys. Rev. A 89, 062102 (2014).
[53] F. K. Kunst, E. Edvardsson, J. C. Budich and E. J. Bergholtz, Phys. Rev. Lett. **121**, 026808 (2018).
[54] Y. Xiong, J. Physics Communications 2, 035043 (2018).
[55] V. M. Martinez Alvarez, J. E. Barrios Vargas, and L. E. F. Foa Torres, Phys. Rev. B 97, 121401 (2018).
[56] Z. Gong, Y. Ashida, K. Kawabata, K. Takasan, S. Higashikawa and M. Ueda, Phys. Rev. X 8, 031079 (2018).

[57] S. Yao, F. Song and Z. Wang, Phys. Rev. Lett. 121, 136802 (2018).
[58] Z. Yang and J. Hu, Phys. Rev. B 99, 081102 (2019)
[59] M. Ezawa, Phys. Rev. B 98, 045125 (2018).
[60] K. Kawabata, K. Shiozaki, M. Ueda, M. Sato, cond-mat/arXiv:1812.09133.
[61] See Supplemental Material II at [xxx] for analytic formulas to understand the LDOS.
[62] See Supplemental Material I at [xxx] for more details on the chiral index (2) and the non-Hermitian winding number.
[63] See Supplemental Material III at [xxx] for the derivation of $t_A^{\pm}$.
[64] See Supplemental Material IV at [xxx] for more details on the skin states and the topological corner mode in rhombohedron geometry of the diamond lattice.
[65] T. Liu, Y.-R. Zhang, Q. Ai, Z. Gong, K. Kawabata, M. Ueda, F. Nori, Phys. Rev. Lett. 122, 076801 (2019).
[66] C. H. Lee, L. Li, J. Gong, cond-mat/arXiv:1810.11824.
[67] E. Edvardsson, F. K. Kunst, E. J. Bergholtz, Phys. Rev. B 99, 081302 (2019).